Journal of Cleaner Production 418 (2023) 138035

Contents lists available at ScienceDirect

Journal of Cleaner Production

journal homepage: www.elsevier.com/locate/jclepro

Volumetric mapping and visualization of life cycle assessment results on computer-aided design models

Teodor Vernica [a], Marija Glišić [a,b], Badrinath Veluri [b], Devarajan Ramanujan [a,c,*]

[a] Department of Mechanical and Production Engineering, Aarhus University, 89G-F Katrinebjergvej Aarhus N, 8200, Denmark
[b] Grundfos A/S, Poul Due Jensens Vej, 8850 Bjerringbro, Denmark
[c] DIGIT Centre, Big Data and Data Analytics, Finlandsgade 22, Aarhus N, 8200, Denmark

ARTICLE INFO

Handling Editor: Panos Seferlis

Keywords:
Life cycle assessment
Scientific visualization
Computer-aided design

ABSTRACT

Life cycle assessments (LCAs) are widely used for identifying opportunities for redesigning engineered parts from a sustainability perspective. However, the data representations and results visualizations used in LCAs remain disconnected from those used for engineering design; this makes it challenging to apply results from LCAs towards redesign decision-making. To address this gap, this paper presents a novel voxel-based approach for mapping process-based life cycle inventory data (and consequently LCA results) to three-dimensional CAD models. The proposed approach can be flexibly applied at different resolutions, i.e., part-level, feature-level, and individual voxel-level based on the granularity of information available. Furthermore, it enables volumetric visualization of LCA results directly on the three-dimensional model of the part. A real-world case study on mapping and visualizing LCA results of a shaft and rotor sub-assembly manufacturing process is used for demonstrating the merits and limitations of the proposed approach.

1. Introduction

Life cycle assessments (LCAs) have emerged as a widely used method for evaluating the life cycle environmental impacts of products—from raw material extraction to their end-of-life. Results from LCAs can be used for identifying *environmental hotspots*, i.e., life cycle stages and processes that significantly contribute to the overall lifecycle environmental impacts of a product or system. Comparative LCAs are also useful for benchmarking the environmental impact of products or systems against alternatives providing a similar function. LCAs are typically conducted in four stages: (i) defining the goal and scope of the analysis, (ii) life cycle inventory (LCI) analysis, (iii) life cycle impact assessment (LCIA), and (iv) interpretation of the inventory and impact assessment results. A more detailed explanation of the various steps in performing an LCA is presented in the ISO 14 040 standards series (International Organization for Standardization, 2006).

Integrating LCAs into the design stage is viewed as a critical step in mitigating the potential environmental burdens resulting from producing products (Bernstein et al., 2010). This is due to the fact that designers take significant decisions related to a product's material, geometry, behavior, and performance at the design stage. Thus, from a sustainability perspective, a designer's attention is on defining and identifying product and process features that can mitigate its lifecycle environmental impacts. Considering results from LCAs in the design process adds additional parameters and constraints, thereby increasing the complexity of design decision-making (Ramanujan et al., 2017b). This process is further challenged due to the mismatch in data representations used (and produced) during LCA studies and those required in traditional engineering design (Rio et al., 2013). LCAs are typically constructed from aggregated inventory data (e.g., mass, energy consumption) and do not require information regarding attributes such as part geometry, ordered sequence of operations in manufacturing a part, and resulting part tolerances. Furthermore, results produced by LCAs are also typically aggregated at the level of a functional unit, process, or lifecycle stage. Thus, they further separate the context of the LCA results from the required product or process improvements For example, it can be challenging to identify potential opportunities for redesigning geometric features in a part based on LCA results (Bernstein et al., 2020). LCA results can also be complex-to-interpret due to the fact that they can present multidimensional results that also include significant uncertainties (Chang et al., 2014; Maruschke and Rosemann, 2005; Reap et al., 2008). Given such challenges, effective communication of LCA results to decision-makers has been an active area of discussion (Heijungs, 2014; Prado et al., 2022)

* Corresponding author at: Department of Mechanical and Production Engineering, Aarhus University, 89G-F Katrinebjergvej Aarhus N, 8200, Denmark.
E-mail addresses: teodor.vernica@mpe.au.dk (T. Vernica), marija.glisic@mpe.au.dk (M. Glišić), bveluri@grundfos.com (B. Veluri), devr@mpe.au.dk (D. Ramanujan).

https://doi.org/10.1016/j.jclepro.2023.138035
Received 21 February 2023; Received in revised form 16 June 2023; Accepted 8 July 2023
Available online 13 July 2023

2. LCA visualization

Prior research shows visualization-based methods and visual analytics tools can aid in the interpretation and communication of LCA results, and aid decision-analysis (Ramanujan et al., 2017b,a). Effective communication is critical for integrating sustainability considerations into the design and manufacturing stages (Uchil and Chakrabarti, 2013). Current LCA tools typically output results as spreadsheets and are visualized through generic, mostly static, visualization schemes such as bar charts, pie charts, Sankey diagrams, etc. Cerdas et al. (2017) discuss the various visualization schemes typically employed to visualize LCI/LCA data and their respective capabilities for the context in which they are used. However, while these visualizations may be well suited for the LCA experts who are conducting the studies, non-practitioners e.g., decision-makers such as designers, might lack the experience required to interpret these highly-complex results (Raoufi et al., 2019). Moreover, the presented data and visualizations might simply be unfit as different stakeholders have different goals and needs (Rio et al., 2019).

With this in mind, efforts have been made to develop novel, or specialized visualization schemes and tools to better assess and communicate various aspects of LCI/LCA data to non-experts. For instance, in order to tackle the multi-dimensional aspect of LCA data, previous research proposed the use of dimensionality reduction techniques, such as principle component analysis (Téno, 1999; Gutiérrez et al., 2010). Otto et al. (2003) and Otto et al. (2004) proposed a novel glyph-based visualization scheme to visualize multi-dimensional LCA data, while Lupton and Allwood (2017) proposed a novel hybrid Sankey diagram design to visualize multi-dimensional LCI data and material flows. Cerdas et al. (2017) propose the adaptation and use of cluster heat maps, widely used in other domains, to visualize LCA results across multiple life cycle phases and impact categories. Müller and Hiete (2021) suggest a novel visualization technique to aid decision-makers in choosing between product alternatives that simultaneously satisfy their needs across multiple sustainability dimensions. Bernstein et al. (2015) developed a tool, consisting of multiple mutually coordinated views, for the visualization of the environmental impacts of products and supply chains, for design-related decision-making. Scheve et al. (2022) developed the interactive *Impact Landscapes* visualization scheme designed to facilitate the interpretation and communication of hierarchical LCA data i.e., contribution trees. Other efforts include visualization tools to assess the environmental impact of different materials (together with their material properties) in the preliminary design stages (Saidani et al., 2020), and methods to visualize uncertainty (Chen et al., 2018; Michiels and Geeraerd, 2020). In spite of the previously developed visualization schemes and tools for the various aspects characteristic of LCA data, most approaches still focus on visualizing data aggregated at a product or process level. This is perhaps, as mentioned previously, due to the manner in which LCAs are performed, and the fact that the product geometry, and therefore its features, are seldom taken into account. To the best of our knowledge, no previous efforts have been made to relate environmental impacts to the product geometry for the visualization of environmental hotspots at a high level of granularity.

Similar efforts to visualize environmental impacts have been made in related domains, such as building design and construction (Elbeltagi et al., 2017; Resch et al., 2020; Hollberg et al., 2021). While the overall method and goals are similar, i.e., using LCAs to quantify the environmental impacts of materials, buildings, and related processes, the two contexts differ in many ways, including the tools and data representations used. That said, visualizations developed for the construction sector can be relevant nonetheless, and can potentially inform visualizations for the engineering design (product) domain. In this sense, particularly noteworthy efforts, include visualizing environmental impacts in the context of the three-dimensional geometry of construction sites (Hajibabai et al., 2011) and buildings (Wiberg et al., 2019). Röck et al. (2018a) and Röck et al. (2018b) proposed a method to integrate LCA and building information models (BIM). This allows for an integrated calculation of LCA results and mapping of the resulting emissions to individual building elements such as walls, floors, or windows. Emission values are encoded as color values within the three-dimensional building model. This integration further allows the generation and comparison of alternative scenarios, by comparing the values of the current design, with possible improvements generated by using different materials. Commercial tools such as *One Click LCA*[1] and *Autodesk Insight*[2] further facilitate this BIM-LCA integration and provide designers with visualization tools for environmentally-aware decision-making.

A similar integration between LCA results visualization and design representations is still largely missing within product and process design. This can be observed in the discrepancy in data representations used between LCA practitioners and design and manufacturing engineers. While designers and manufacturers archive product lifecycle using representations such as CAD models, engineering drawings, manufacturing process plans, etc., LCA results are exported as spreadsheets, charts, and reports that are not easily related back to original data representations. Previous research has attempted to integrate LCA and CAD to facilitate the consideration of sustainability within design stages (Ostad-Ahmad-Ghorabi et al., 2009; Tao et al., 2017, 2018). These works mainly focus on integrating life cycle information and design parameters inherently contained in the CAD part definitions (e.g., mass, volume, material definition) to be used for LCA calculations. Gaha et al. (2018) proposed the *eco-feature* concept, where individual CAD features can be extracted and evaluated from an environmental performance point of view. However, the above works lack the visualization perspective needed to communicate the results back to designers. Ostad-Ahmad-Ghorabi et al. (2009) presented a conceptual methodology for relating and visualizing LCA results with CAD. The authors liken the proposed LCA visualization to the current integration of finite element analysis into CAD systems. In their view, LCA results would be encoded through a color scheme of the components of the CAD model. As the proposed concept aggregates LCA results visualization at the product level, it does not accurately visualize impacts from processes that operate on specific features and geometric regions of the product. In other words, the environmental impacts from a manufacturing operation such as drilling a hole would be attributed to the entire component, and not the hole itself. Moreover, simply mapping LCA results to the final CAD model of the component omits important context in the form of the intermediate steps and transformations that a product goes through from raw materials to the finished part. A similar component-level LCA integration has since been implemented in commercial CAD tools such as *Solidworks Sustainability Xpress*.[3]

3. Research objectives

The overarching goal of this research is to address the disparities in data representation models and visualizations between LCA and those used in engineering design. Specifically, this work aims at adding geometric context to LCA studies by linking them to three-dimensional CAD models of products. While the methods proposed in this paper can be extended to other product types and lifecycle stages, it is an open question as to whether visualizing LCA results on three-dimensional CAD models is meaningful in such contexts.

Different from prior work (see Section 2) that only focus on mapping final results from LCAs to CAD models, this work develops a physically-valid methodology for mapping LCI data in process-based LCAs to

[1] https://www.oneclicklca.com/.

[2] https://www.autodesk.com/products/insight/overview.

[3] https://www.solidapps.co.uk/products/products-solidworks-simulation/products-sw-sustainxpress.

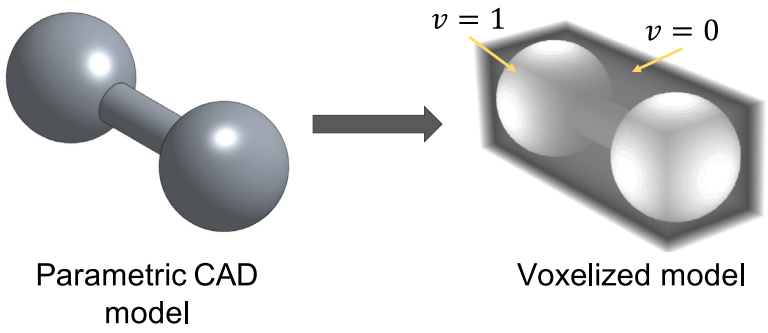

Fig. 1. Voxel-based representation of parts. The semi-transparent gray box illustrates voxels (v) set to zero in the 3D grid representing the voxel space. Voxels contained in the part volume are set to 1 and illustrated in white.

product geometry. It is worth noting that linking LCI data to detailed product and process information has been an area of active research, e.g., developing parametric unit process life cycle inventory models for manufacturing processes (Raoufi et al., 2020; Thoft Krogshave et al., 2020; Boettjer et al., 2021). At the cost of requiring additional product life cycle information, the benefit offered by the above models is more accurate modeling and parameterization of LCI data, as well as identifying the sensitivity of LCI data to product and process information. Motivated by these works, our methodology aims to enrich the interpretation of LCI data and consequently LCA results by adding geometric context.

The contributions presented in this paper include a generalized methodology for mapping LCI data and LCA results to three-dimensional part geometries. The formulated method can be flexibly applied at different levels of resolution, i.e., part-level, feature-level, and sub-feature-level depending on the granularity of LCI information available. The paper also discusses the use of this mapping methodology for creating three-dimensional volumetric visualizations of LCI and LCA results directly on part geometries. The produced volumetric visualizations are physically-valid, i.e., summing the value of the visualized LCI or LCA results over the product volume accurately reproduces the overall results. The produced visualizations also encode physical causalities resulting from chaining unit processes, including processes that transform the part geometry. To demonstrate the application of the mapping and visualization techniques, the paper presents a case study that visualizes the cradle-to-gate impacts for manufacturing a shaft and rotor sub-assembly.

4. Methodology

Process-based LCIs quantify energy and material exchanges for a set of unit processes (within the scope of the LCA study) using direct measurements or using commercial LCI databases. Herein, inventory data and the resulting environmental impacts are typically quantified on a unit mass basis (e.g., producing a 1-kilogram injection molded plastic component, transporting a 1-tonne product by 1 kilometer) or a unit volumetric basis (i.e., per volume, surface area, etc.). Thus, a volumetric representation of product geometry can be directly and intuitively mapped to LCI data and LCA results at any arbitrary scale of resolution. To this end, our proposed method uses a volumetric representation for part geometries and maps LCI data and LCA results to individual *unit volumetric elements* also termed as *voxels*. Further details are presented in the sections below.

4.1. Voxel-based representation of part geometry

In the current work, the three-dimensional geometry of a part is represented in voxel space, which is defined as a three-dimensional grid or lattice of voxels (Kaufman et al., 1993). A voxel is a three-dimensional discrete unit of volume and is conceptually analogous to a pixel. Therefore, a voxel has a predefined but arbitrary size and fixed shape. For representing a part in voxel space, we define a $I \times J \times K$ grid, where I, J, and K define the total number of voxels in each of the three dimensions. Next, as shown in Eq. (1), the value of a voxel v is set to 1 if the voxel lies within the geometric volume V of the part. Otherwise, the value of that voxel v is set as 0. This creates a discretized representation of the part geometry in binary voxel space as illustrated in Fig. 1.

$$v \begin{cases} 1, & \text{if } v \in V \\ 0, & \text{otherwise} \end{cases} \tag{1}$$

Voxel-based representations have previously been leveraged for CAD applications such as prosthesis design (Jense, 1989), geometric modeling (Chandru et al., 1995), printability assessment (Telea and Jalba, 2011) for additive manufacturing, and thickness analysis of complex shapes (Patil and Ravi, 2005). Our primary motivation for utilizing a voxel-based representation for part geometries follows from the fact that the discretization of part geometry through voxelization serves as a useful analogy for mass subdivision. By definition, voxels have a fixed volume (and shape) and consequently represent a conserved quantity of mass. Thus, by subdividing the part geometry into a set of voxels, LCI and LCA results for a specific unit process can be allocated to corresponding voxels using a mass-based allocation. Furthermore, voxel-based representations enable visualization of scalar quantities (such as LCI and LCA results) directly on the corresponding part volume (Xue et al., 2016). It is worth noting that a voxel space discretizes a continuous geometric representation and therefore represents an approximation of the original geometry. The accuracy of this approximation is a function of the chosen density of the voxel space or in other words, the number of voxels (I, J, K) along each dimension. A higher voxel density increases the accuracy of the geometric approximation and can also increase the information density of volumetric visualizations. In practice, the selection of voxel density is constrained by the availability of computational memory and power.

4.2. Overall workflow for mapping LCI/LCA results to voxel models

An overview of the workflow for allocating LCI/LCA data for a given part or assembly is illustrated in Fig. 2 and described below.

1. **Obtain process plan and identify unit processes** - First, unit processes and their sequence of operation need to be identified from existing process plans. The processes are subsequently classified according to Table 1 to determine the corresponding LCI/LCA allocation methodology.
2. **Collect CAD data** - CAD models of the part or assembly are collected for the voxelization process. Although not strictly necessary, *pre* and *post* models of a part can be collected for cases where there is a change in geometry. These intermediate models facilitate the data allocation process, though the change in geometry could also be modeled through other means.

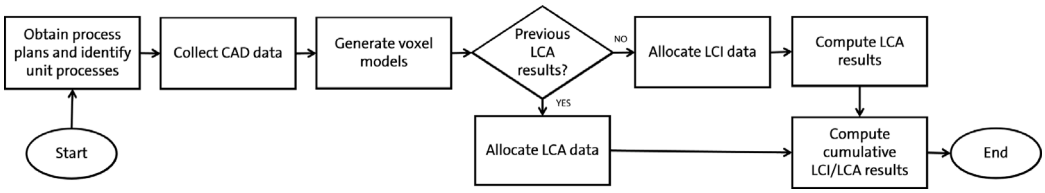

Fig. 2. A high-level overview of the workflow for allocation LCI/LCA data to voxel-based data.

3. **Generate voxel models** - Voxel models are generated based on the previously collected CAD models, using a voxelization algorithm, such as those presented in Patil and Ravi (2005). A suitable resolution for each voxel model must be chosen at this stage. Naturally, there is a trade-off between resolution and performance. Therefore, the resolution should be chosen to adequately capture all of the necessary geometric features of the part while preserving reasonable performance for generating and updating the models.
4. **Allocate LCI from unit processes to voxel models** - LCI data for each unit process is allocated to corresponding regions of the voxel models based on the identified process class in Step 1. This allocation process is detailed in Section 4.3. In certain cases, additional information regarding the process may be needed to inform the allocation process e.g., the depth to which a surface treatment should be made.
5. **Compute LCA results through LCIA** - LCA results are computed based on the LCI values previously allocated to voxels. If results from prior LCA studies are available, then the LCI allocation step can be skipped and LCA results are directly allocated to voxel models following the same allocation formulae outlined in Section 4.3.
6. **Compute cumulative LCI/LCA results** - Cumulative LCI/LCA results are computed based on the process order, i.e., allocation order, as explained in Section 4.4.

4.3. Generalized allocation model for voxels

The fundamental idea behind this paper is allocating LCI and LCA data to a voxel-based representation of part geometries. The generalized model for allocating LCI (or LCA data) to voxels is given below in Eq. (2).

$$L_{i,v} = L_i \cdot s \cdot \frac{f_{i,v}}{\sum f_{i,v}}; v \in V \tag{2}$$

Here,

- $L_{i,v}$ is the ith LCI parameter or impact category result for a unit process, allocated to each voxel v.
- s is the scaling factor by which the unit process is scaled and represents the demanded quantity of the unit process.
- L_i is the ith LCI parameter or impact category result for the unit process.
- $f_{i,v}$ is the fractional allocation of L_i for the voxel v in order to achieve the necessary change in geometry and/or material properties.
- V is the set of all voxels operated upon by the process.

As shown, the LCI or LCA results allocated to a specific voxel are proportional to the work done on that voxel in a specific unit process. To accommodate the different types of volumetric and geometric transformations that occur along unit processes in the lifecycle, we extend the above formulation to a structured classification of unit processes shown in Table 1. This classification builds on the Allen and Todd classification scheme for manufacturing processes as it is closely related to shape transformation (Sorensen et al., 2018). Based on volumetric and/or geometric transformations we classify unit processes into five classes. Within this scheme, our focus is primarily on allocating results to the final part geometry at the end of the manufacturing stage. Operations that occur downstream of manufacturing (e.g., transportation, use-phase, recycling, remanufacturing) can similarly be classified according to Table 1 and allocated back to the part geometry. For instance, a closed-loop recycling process can be categorized as a Class II process, and the credits are allocated back to the final part geometry. However, a specific mapping scheme for operations downstream of manufacturing is out of the scope of this work, and will be explored in the future.

Table 1
Classification of common unit processes for mapping LCI data to a voxel-based representation of part geometry.

Class	Name	Illustrative processes
Class I	Mass conserving & Geometry preserving	Transportation, Heat treatment
Class II	Mass conserving & Reshaping	Forging, Extrusion, Recycling
Class III	Mass reducing & Reshaping	Machining, Stamping
Class IV	Mass adding & Reshaping	Welding, Adhesion
Class V	Surfacing & Geometry preserving	Washing, Electroplating, Hardening

The following subsections detail the application of the allocation methodology to specific classes of unit processes. Please note that the equations in these subsections present the allocation of LCI results to voxels, depending on the unit process classification presented in Table 1. LCA results can be allocated to voxels in one of two ways. LCA results for each voxel can be computed from the allocated LCI results and a chosen LCIA method. Alternatively, if LCA results are directly available (and visualization of LCI results is not needed), the equations presented in this section (Eqs. (3)–(7) can be directly applied to allocate each impact category result (in place of the LCI parameter).

4.3.1. Class I: Mass conserving & geometry preserving

In Class I unit processes, both the volume (mass) and the geometry of the processed part are considered to be unchanged. As Class I unit processes do not selectively operate on the geometry of the part, the proportional work done is considered to be equal for all voxels operated upon by the unit process, i.e., $f_{*,v} = 1$. Thus, the LCI data is equally allocated to all such voxels. Eq. (3) describes the mathematical formulation for this allocation.

$$L^I_{i,v} = \frac{L^I_i \cdot s}{|V_I|}; v \in V_I \tag{3}$$

Here,

- $L^I_{i,v}$ is the ith LCI parameter for the Class I unit process, allocated to each voxel v in the set of non-zero voxels V_I operated upon by that Class I unit process.
- s is the scaling factor by which the Class I unit process is scaled. For most Class I unit processes, this is either the total mass or the volume of the part
- L^I_i is the ith LCI parameter for the Class I unit process.
- $|V_I|$ is the cardinality of the set V_I.

4.3.2. Class II: Mass conserving & reshaping

Class II unit processes conserve the total mass (volume) of the part. Therefore, the total number of non-zero voxels in the voxel space remains unchanged. However, these processes result in reshaping the part, which means the location of a non-zero voxel in the voxel space can be altered by the process. We further assume there is no appreciable change in the density of the material during a Class II unit process. If there is perfect geometric information on a Class II unit process, then information regarding the overall work done on each voxel by that unit process is available. For the sake of generality, this information is specified as a scalar field ϕ, that encodes the variation in work done over the analyzed geometry. In some cases, a physical proxy (e.g., strain energy density) can be estimated using numerical approaches such as finite element analysis that approximate the variation in work done over the analyzed geometry. Eq. (4) describes our formulation for allocating LCI results in these cases. In cases where such detailed information is not available, the Class II process is treated as a Class I process, and the LCI data are evenly allocated.

$$L_{i,v}^{II} = L_i^{II} \cdot s \cdot \frac{\phi_{i,v}}{\sum \phi_{i,v}}; v \in V_{II} \tag{4}$$

- $L_{i,v}^{II}$ is the ith LCI parameter for the Class II unit process, allocated to each voxel v in V_{II}, the set of non-zero voxels operated upon by the Class II process.
- L_i^{II} is the ith LCI parameter for the Class II unit process.
- s is the scaling factor by which the Class II unit process is scaled.
- $\phi_{i,v}$ is the average value of a scalar field ϕ_i within the bounds the vth voxel. The scalar field ϕ_i encodes information (e.g., strain energy density field) on the relative magnitude of work performed on the vth voxel by the Class II process.

4.3.3. Class III: Mass reducing & reshaping

Subtractive processes that reduce the mass of a part and consequently result in a geometry change are classified within Class III. As material is removed from the original part, the number of non-zero voxels in the voxel space reduces after the operation. Consequently, this process creates a new feature (i.e., hole, groove, surface) on the part geometry. As the work done in such processes is a direct function of the material removed, the LCI data is directly allocated to the voxels removed in a Class III operation. Eq. (5) details the specific allocation process used.

$$L_{i,v}^{III} = L_i^{III} \cdot s \cdot r_{i,v}; v \in V_{III} \tag{5}$$

- $L_{i,v}^{III}$ is the ith LCI parameter for the Class III unit process, allocated to a voxel v that belongs to the set of voxels V_{III} removed by that process. V_{III} can be computed by comparing the voxelized part geometry before and after the process.
- L_i^{III} is the ith LCI parameter for the Class III unit material removal process.
- s is the scaling factor by which the Class III unit process is scaled.
- $r_{i,v}$ represents the fractional allocation of L_i to a specific voxel v such that $\sum_{v \in V_{III}} r_{i,v} = 1$. If data on $r_{i,v}$ is unavailable, L_i is considered to be equally distributed among the voxels operated upon in the process (V_{III}), i.e., $r_{i,v} = \frac{1}{|V_{III}|}$.

4.3.4. Class IV: Mass adding & reshaping

This paper distinguishes between two subclasses of mass-adding processes for the purpose of generating volumetric visualizations. The first subclass includes mass-adding processes where a base material is altered (e.g., by melting, fusing, photo-solidification) to produce the desired geometry. Examples include common additive manufacturing processes such as fused deposition molding, powder-based manufacturing, and stereolithography. Such processes are classified as Class II processes as they can be considered mass-conserving processes that reshape/fuse a primary material into a final form.

The second subclass includes joining processes where, two disjointed components are joined thermally, mechanically, or chemically. For these joining processes the LCI for the joining operation is either allocated to, (i) common (or contacting) voxels shared between the two previously disjointed parts, or (ii) contacting voxels between the disjointed parts and the fastener, if the fastener is also treated as a mechanical part. Eq. (6) details this allocation process.

$$L_{i,v,p}^{IV} = L_i^{IV} \cdot s \cdot \frac{U_p}{\sum_{k \in P} U_k \cdot |V_p|}; v \in V_{IV} \tag{6}$$

Here,

- $L_{i,v,p}^{IV}$ is the ith LCI parameter for the Class IV unit process and is allocated to a non-zero voxel v that is on the surface of the pth part, and belongs to the set of surface voxels V_{IV} representing all contacting/common voxels operated upon by the Class IV process.
- s is the scaling factor by which the Class IV unit process is scaled.
- U_p is the total volume of the contacting/common belonging to the part p that is operated upon by the Class IV process.
- $\sum_{k \in P} U_k$ represents the summation of the total volume of the contacting/common voxels across the set of all parts P operated upon by the Class IV process.
- $|V_p|$ represents the cardinality of the subset of voxels in V_{IV} belonging to the part p.

4.3.5. Class V: Surfacing & geometry preserving

Class V processes operate on the surface of a part without leading to a significant change to the geometry of the part. Depending on the application, surface processes such as painting, or electroplating could be classified under Class V processes (i.e. mass added can be neglected). Eq. (7) details this LCI allocation for Class V processes.

$$L_{i,v}^{V} = L_i^{V} \cdot s \cdot \delta(v); v \in V_V \tag{7}$$

Here,

- $L_{i,v}^{V}$ is the ith LCI parameter for the Class V unit process and is allocated to a voxel v from the set of non-zero voxels operated upon by the Class V process (V_V).
- L_i^{V} is the ith LCI parameter for the Class V unit process.
- s is the scaling factor by which the Class V unit process is scaled.
- $\delta(v)$ represents a depth function that models the relative allocation of L_i^V based on the operating depth of the Class V process. For example, if a surface hardening process uniformly changes the hardness of the part to a depth of d units, then $\delta(v) = 1/|S|$ for $v \in S$ and $\delta(v) = 0$ otherwise. Herein $S \subset V_V$, and is defined as voxels in V_V whose centroid is at most d deep from the part surface.

4.4. Computation of cumulative LCI & LCA results

Sections 4.3.1–4.3.5 define the procedure for allocation of LCI results to corresponding voxels for a unit process belonging to classes I-V. In reality, the lifecycle of parts is composed of multiple, sequential unit processes. Therefore, in order to compute cumulative LCI results, the LCI parameters allocated to each voxel need to be aggregated over a series of unit processes.

The computation of cumulative LCI results for a voxel v follows the superposition principle, i.e., $\sum_i^N L_{i,v}^* = L_{1,v}^* + L_{2,v}^* \cdots L_{N,v}^*$. Here, $L_{i,v}^*$ is the ith LCI parameter for a unit process of a generic class $*$.

Cumulative LCI results for each voxel v are computed sequentially, as the composition of unit processes operations that modify the part geometry is not necessarily commutative. In other words, cumulative LCI results $\sum_i^N L_{i,v}^*$ for each LCI parameter is computed in the exact sequence of the unit processes $L_{1,v}^* \rightarrow L_{2,v}^* \cdots \rightarrow L_{n,v}^*$.

The cumulative LCI results obtained for each voxel in the part can be converted to LCA results based on a user-specified LCIA methodology. Alternatively, as discussed earlier, externally computed LCA results can be allocated directly to the part geometry, based on the process classification methodology in Table 1 and Eqs. (3)–(7).

5. Visualization methodology

The data allocation methodology presented above contextualizes LCI/LCA data within the three-dimensional space of the manufactured part. Among other possible use cases, this enables the generation of three-dimensional data visualization schemes. However, while there is a clear, objective mapping from LCI/LCA data to the part geometry, it is not necessarily ideal for interpreting and analyzing results from a human decision-making perspective as is. These data need to be further processed to be visualized, and there is no unique way to do so.

Finding the optimal visualization approaches (e.g., volume rendering techniques (Meißner et al., 2000), multi-dimensional visualization approaches (MacEachren et al., 2003)) for different scenarios is beyond the scope of this work. Instead, we propose one such visualization scheme to illustrate the usefulness of the allocation methodology developed in Section 4. The visualization design aims to highlight the environmental impacts of creating specific geometric features on the analyzed part. We motivate the design decisions to achieve this goal in the remainder of this section and discuss the most critical aspects required to obtain physically-valid visualizations and overcome some of the typical drawbacks of three-dimensional visualizations.

5.1. Data encoding channels

Once allocated, LCI/LCA data needs further processing to visualize the results. Like other visualization methods (e.g., choropleth maps) each mark, here voxels, must be mapped to visual channels based on their value and a chosen visualization scheme. For instance, colors can be mapped to voxels by linearly interpolating between two color values based on each voxel's value in relation to the minimum and maximum values present within the part model. It should be noted that the voxel-based representation imposes some inherent constraints on the possible visual channels used to encode data. Firstly, voxels are inherently constrained in channels such as volume, shape, or angle. Using these channels would go against the definition of a voxel and would not preserve the original geometric representation of the model. Secondly, voxels already leverage the three positional channels to encode positional data. This leaves channels such as color hue, saturation, luminance, texture, or transparency as some of the only viable options.

The choice of colors, interpolation scheme, classed vs. unclassed color scales, etc. are subjective choices that need to be considered based on the intent of the visualization, data distribution, and others. In this work, the intent of the visualization is to showcase the overall distribution of the allocated LCI/LCA data per manufactured features. For this, we utilized a classed, jet color map to clearly distinguish between impact value classes.

5.2. Visualization of removed voxels

In cases where a voxel v is removed (i.e., $v : 1 \rightarrow 0$) by a mass-reducing operation, our visualization design allocates the cumulative LCI/LCA results for the removed voxel to corresponding non-zero voxels on the surface of the feature created by that mass reducing operation. This re-allocation process is necessary to ensure the conservation of the total LCI/LCA allocated to visible voxels. Moreover, it aims to generate a physically accurate visualization that represents results for the entire process required to create a feature, including the necessary preceding operations.

The choice of the specific allocation method is subjective, and the main aim is to support human interpretation of the displayed results. For example, a distance-based weighting function $D(v_s, v_r)$ can be used to determine the allocation of LCI/LCA data to a non-zero voxel on the surface of the feature (v_s), based on its distance from a removed voxel (v_r). The specific formulation of this function can be determined based on the sensibility of the resulting visualizations. In this work, LCI/LCA values from one or more removed voxels are equally distributed to the immediately neighboring visible voxels. This process will be further exemplified in Section 7. Future work should investigate the alternative ways of redistributing this data, through other weighting functions, for effective results communication.

5.3. Visualization of occluded voxels

By the nature of mechanical processes, most operations act on the surface of a part, thus facilitating visualization on a three-dimensional model. However, that is not always the case, and our methodology allocates data within the volume of the part, based on the features created by a unit process. This poses a visualization challenge for voxels occluded by surface voxels. Adjusting the transparency value of voxels can be used to mitigate this issue and present a more complete depiction of the data. While partial transparency might pose a challenge in itself due to many compounding layers of transparency, invisibility (i.e., full transparency) can be effectively used to visualize, and even highlight areas of interest. This allows the visualization of data attributed to interior sections of a part or assembly, by simply iterating through the voxels and hiding them based on a given threshold on the I, J, and K dimensions of the voxel model. To this end, established isosurface rendering techniques (Newman and Yi, 2006) can be leveraged, given the discrete, volumetric representation.

5.4. Variable voxel density model comparison

If voxels are colored based on the value allocated to them, special attention needs to be given when comparing two or more models of different voxel densities. This is because LCI and LCA results associated with creating a feature of the part geometry are distributed among the voxels comprising said feature. Therefore, the value attributed to a voxel is inversely proportional to the voxel density of the model. This is not an issue if the two models are voxelizing an equal volume and have the same resolution as defined in Section 4.1. However, for efficiency purposes, it can be useful to only voxelize the volume necessary for the given model, or voxelize models at different resolutions resulting in different voxel densities. In such cases, values need to be normalized to the same unit measure to be accurately compared, e.g., kg. CO_2 emissions per cm^3. This can be obtained by simply dividing the LCI/LCA data allocated to each voxel value by the volume of that voxel.

6. Software implementation

To demonstrate the applicability of our methodology using a case study, we developed an application in the Unity[4] engine. The application makes use of Unity's 3D development environment to generate an interactive voxel-based visualization. The general structure of the implementation and its interactions are illustrated in Fig. 3 and further explained below.

Input data - The necessary data for the implementation consists of CAD models, process plans, and LCI/LCA values. CAD models of the components are used to generate the corresponding voxel-based representation and inform the selection of relevant voxels for allocation. Process plans are similarly used to inform this selection process, while the LCI/LCA values are allocated to relevant voxels.

Voxel-based representation - A voxel-based representation is generated based on the input CAD model of a component using available tools.[5] The representation is generated as a three-dimensional matrix of voxels. Voxels are stored as a data structure (Listing 1) containing its I, J, and K indexes within the matrix, its visibility value (i.e., 0 or 1), and an array of values corresponding to the allocated LCI parameters

[4] https://unity.com.

[5] https://github.com/mattatz/unity-voxel.

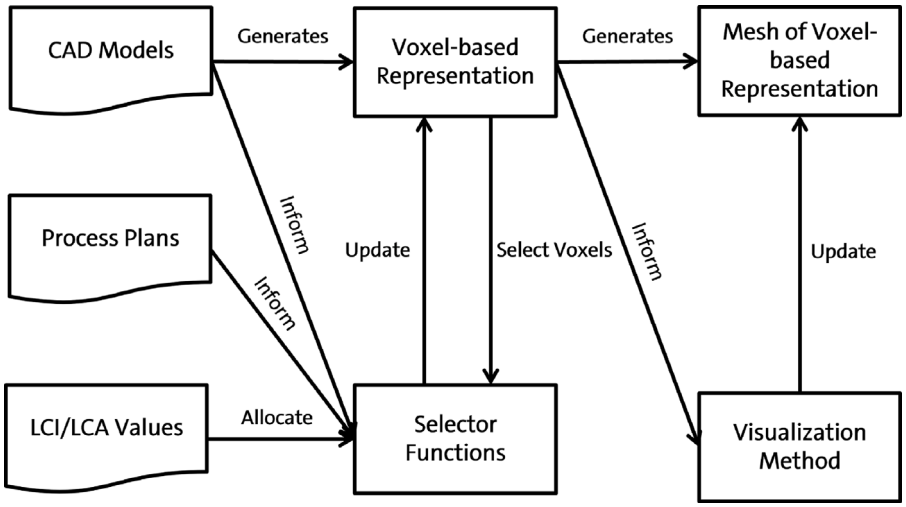

Fig. 3. Software implementation structure.

or LCA indicators. It should be noted that the class could be extended to incorporate additional parameters such as uncertainties in LCI/LCA results or material properties.

Mesh of voxel-based representation - A three-dimensional mesh is generated based on the voxel-based (matrix) representation in order to visualize it. Vertices and faces are generated corresponding to each visible voxel within the voxel matrix, forming a mesh of the entire representation. It should be noted that the voxel-based representation is a data structure, independent of the mesh generated to visualize it.

Selector functions - Selector functions are designed and implemented to select relevant voxels from the entire representation. The output of a selector function is a set of voxels, which can then be used to allocate the corresponding LCI/LCA values, according to the presented methodology. The selector functions can be informed by the part design (e.g., feature position, dimensions, and type), to select the voxel regions corresponding to part features. The data allocation process for the selected voxels is performed sequentially, per unit process; process plans are therefore used to inform the order of the selector functions. The functionality of selector functions can be as simple as selecting all voxels (e.g., for uniform allocation for a Class I process), selecting all surface voxels from a particular direction (e.g., for a Class V process allocation), or be arbitrarily complex in order to model more specialized unit processes and/or geometries. Given that the output of a selector function is a set of voxels, multiple functions can be combined by using set operations (e.g., intersection, union, difference) on their output, achieving more complex selections from simple primitives.

Visualization Method - The visualization method defines and controls the look of the voxel mesh, to visually communicate the allocated results. Here, the number of colors, the color values, whether these should be classed or not, and the interpolation scheme are defined. Vertices and faces in the mesh representation are colored, based on the value allocated to each corresponding voxel in the voxel matrix and the parameters defined in the visualization method.

Listing 1: Voxel class structure.

```
Class Voxel
{
    int                 I, J, K
    bool                IsVisible
    array of double     Values
}
```

7. Case study

To demonstrate our methodology, we conducted a case study on a real-world *shaft and rotor* sub-assembly of an electric motor. The case study was done in collaboration with an industrial partner and made use of internal data provided by the manufacturer. The case study serves to verify the applicability of the proposed methodology towards mapping and visualizing cradle-to-gate LCA results onto part geometries using data that is available in industrial settings. Evaluating the efficacy of the generated visualization schemes is out of the scope of this case study and will be presented in future work. The presented data have been normalized for confidentiality reasons, without affecting the interpretability of the results. The sub-assembly was chosen to illustrate the visualization methodology on a reasonably complex component undergoing a series of geometry-altering processes. Moreover, the context of an assembly allows for comparatively evaluating the manufacturing impact of individual features across multiple components and visualizing the impact of assembly processes that can be attributed to more than one component. This also allows the demonstration of the allocation methodology applied to a variety of unit processes of different classes.

7.1. Sub-assembly description

Fig. 4 displays the CAD models of the components imported by the manufacturer to produce the *shaft and rotor* sub-assembly. These consist of (from left to right) a round bar, a laminated rotor stack, magnets, and end covers.

Fig. 5 illustrates the unit processes applied to the four components and their sequence of operation. The round bar undergoes a series of material removal processes. First, the bar is cut to the design-specified length, followed by a drilling operation at the top and bottom surfaces of the round bar. Then, two turning operations reduce the diameter of the bar to various sizes across its length. A milling operation is then employed to produce a keyway. Finally, the shaft undergoes a grinding operation at two locations. Magnets are glued and inserted into the slots within the laminated rotor stack. End covers are punched from a metal strip. Lastly, the end covers are placed onto the rotor stack with magnets and the finished shaft is pressed inside. The *upstream processes* elements in the figure encapsulate operations that the components underwent, from material extraction to arriving at the manufacturer in their current state.

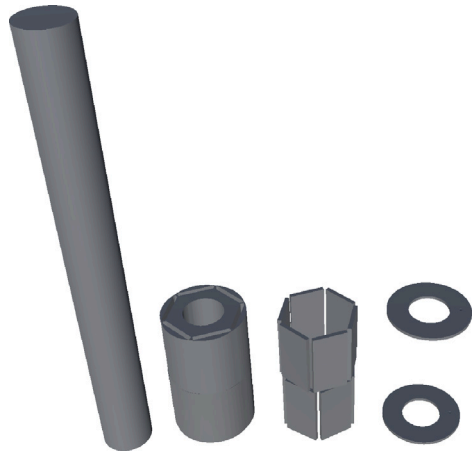

Fig. 4. CAD models of the components imported by the manufacturer to produce the shaft and rotor sub-assembly: round bar, laminated rotor stack, magnets, and end covers.

Table 2
Normalized LCA results for producing the *shaft and rotor* sub-assembly.

Component	Process	Normalized results (kg. CO_2 eq.)
Shaft	Manufacturing	0.190
Shaft	Cutting	0.017
Shaft	Drilling	0.003
Shaft	Pre-turning	0.210
Shaft	Turning	0.023
Shaft	Milling	0.002
Shaft	Grinding	0.022
Laminated rotor stack	Manufacturing	0.323
Magnets	Manufacturing	1
End covers	Manufacturing	0.053
End covers	Punching	9E−05
Rotor stack w/ Magnets	Insertion	0.003
Shaft and Rotor sub-assembly	Pressing	0.048

7.2. LCA study

A cradle-to-gate LCA study was conducted using internal data from the manufacturer to assess the environmental impacts of producing the *shaft and rotor* sub-assembly. Please note that the results are normalized to preserve data confidentiality. The conducted LCA used the Ecoinvent 3.6 and GaBi 2020 LCI databases to model the processes described in Fig. 5 as it was not possible to collect primary data from the production line. The ReCiPe 2016 Midpoint (H) impact assessment method (Huijbregts et al., 2016), was used to compute the environmental impacts of the production process. For conciseness, this case study illustrates the proposed methodology for allocating and visualizing LCA results using the *global warming* impact category. The methodology would be identical if applied to other midpoint impact categories.

Table 2 presents the results of the LCA study for the global warming impact category. As shown, results were estimated per unit process, with the exception of the upstream processes (i.e., extraction and production of raw materials).

7.3. Methodology implementation

Given the required input data, the workflow described in Section 4.2 was implemented to allocate the LCI results to corresponding component geometries. First, unit processes were identified based on the process plans. The processes were then categorized based on the classes from Table 1. Table 3 shows the classification of the processes involved in the sub-assembly manufacturing process. CAD models of the components, shown in Fig. 4, including intermediate stages, and final parts were collected. Then, voxel models were generated as described in Section 6 based on the collected CAD models, with variable resolutions (measured in mm^3 per voxel), as follows: shaft - 0.59; rotor stack - 0.65; magnets - 0.61; and covers - 0.75. As LCA data was directly available, the LCI allocation step was skipped and LCA results were directly allocated to the components (see Section 4 for details). Data was allocated sequentially, per unit process, based on the operations shown in Fig. 5.

Table 3
Case study unit process classification.

Process	Class	Comments on allocation
Cutting	III	Data is allocated uniformly among all removed voxels, then redistributed to visible surface voxels in the resulting features created in the processes.
Drilling	III	
Pre-turning	III	
Turning	III	
Milling	III	
Punching	III	
Grinding	V	Data is allocated to the surface voxels ($d = 1$).
Insertion	IV	Data is allocated to contacting surface voxels between the magnets and rotor stack components.
Pressing	IV	Data is allocated to contacting surface voxels between the shaft, rotor stack with magnets, and end cover components.

Fig. 6 exemplifies the data allocation process for the milling process responsible for creating a keyway feature on a shaft. First, the LCA value allocated before the milling process x_0 is shown to be evenly distributed among the 55 (light gray) voxels. Second, voxels corresponding to the future keyway are identified through a selector function. In this case, voxels are identified by generating a voxel-based representation of the shaft before and after the creation of the feature (based on the CAD models). The difference between the two models, m_1 and m_2 can be computed by applying an *exclusive or* (XOR) binary operation on the visibility values v of voxels i from the two models according to Eq. (8). Voxels for which the resulting value r is 1 correspond to ones forming the keyway feature. Once voxels are selected, the LCA impact value of the milling operation is distributed according to Eq. (5). In Fig. 6 example, the milling LCA value x_1 is distributed and added to the 23 (red) voxels to be removed. Third, as this is a material removal operation, the total value allocated to the selected voxels (including any previously allocated value) x_2 is stored before being removed, and the visibility of the voxels is set to 0. Finally, the stored value x_2 is redistributed to the 20 nearest neighboring visible voxels (dark gray).

$$r_i = v_i^{m_1} \oplus v_i^{m_2}; v \in \{0, 1\} \tag{8}$$

8. Results

With the complete LCA study, results are mapped to the component geometry according to the methodology. Fig. 7(a) shows the final results of the mapping and highlights the data distribution at a feature-level. Voxel regions are colored based on the minimum and maximum voxel values contained between all components of the sub-assembly. To better highlight the differences, colors are assigned based on their Log_{10} values. Given that colors are linearly interpolated between the minimum and maximum values, this ensures that outliers do not heavily skew the use of colors towards one end of the scale. Fig. 7(b) shows the same results with the assembled components, and Fig. 7(c) shows a cross-section view of the final feature-level results, which allows the visualization of the impact allocated to interior features, such as the drill holes. Naturally, the information density present within the voxel representation varies between the surface and interior voxels. This is particularly true for the shaft, where most of the unit processes operate on the part surface, thus where most of the information is allocated.

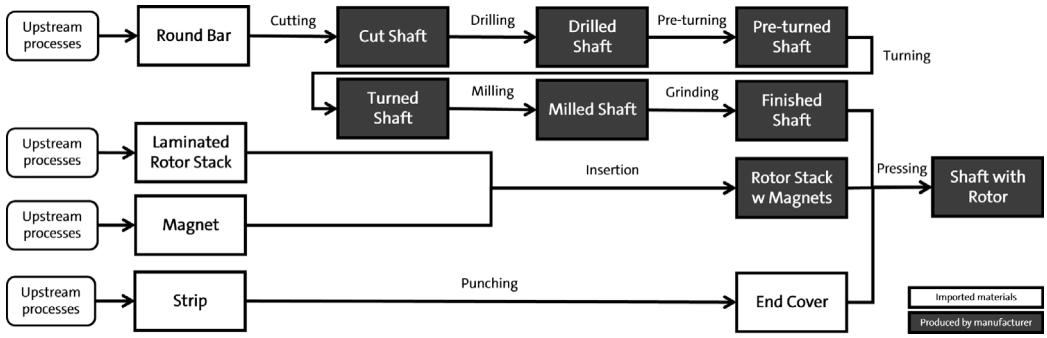

Fig. 5. Process diagram showcasing the materials and sequence of operations used to obtain the final *Shaft with Rotor* sub-assembly.

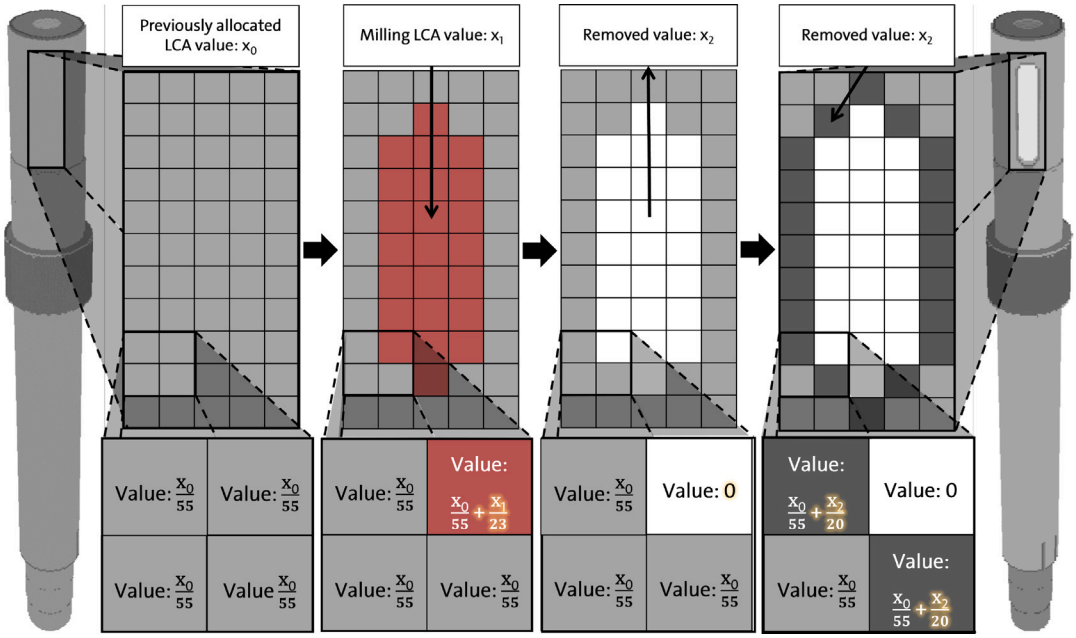

Fig. 6. Two-dimensional data allocation example for a milling (i.e., Class III) process. Here, red squares represent voxels identified by the selector function to be removed. White squares represent invisible voxels. Dark gray squares represent voxels with a higher allocated LCA value compared to the base, light gray, squares. Note that changes in voxel values between steps are highlighted in yellow.

In contrast, Figs. 7(d)–7(f) illustrate the same results at a component-level. This is done by assigning all voxels of a component the same color value, based on the global warming impact allocated to each component in the sub-assembly. This visualization scheme can be useful in distinguishing the overall environmental impact of components, but much of the geometric context is lost. In other words, using this visualization scheme makes it obvious that the magnets have the highest global warming environmental impact in the sub-assembly. However, all information regarding the component's features is lost, along with any indication of the contributions of specific processes or geometric features. Thus, this resulting visualization is equivalent to uniformly allocating all data to the finished component (Class I process), resulting in a more information-sparse visualization.

Fig. 8 shows the series of material removal processes (presented in Fig. 5) applied to the round bar voxel model, transforming it to the final shaft. The respective impact calculated for each unit process is allocated sequentially. As described in Section 5, in the case of a material removal process (Figs. 8(c)–8(f)), LCA data is first attributed to corresponding voxels. Then, any value previously attributed to removed voxels is transferred to the closest non-removed voxel as previously exemplified in Fig. 6. The sequential allocation of LCA data per unit process allows the progressive visualization of the impact of the component across intermediate stages. Please note the colors and legend values in the figure change based on each new assignment.

Fig. 8(g) shows the evolution of voxel values for three of the most impactful shaft features, allocated across all modeled processes. For instance, the top shaft surface (a), is allocated a relatively high value per cm^3 during the cutting process (Fig. 8(b)), but remains constant thereafter, as no other subsequent process affects (and therefore allocates to) the same set of voxels. The reason behind the high impact per cm^3 is that LCA calculations typically consider the volume of removed material, rather than the feature created. Therefore, the impact value that would otherwise be attributed to the volume of removed material is here projected to a pseudo-two-dimensional surface, i.e., the top voxel layer. In contrast, the top bearing surface (b) is initially allocated a lower value per cm^3 during the pre-turning process (Fig. 8(d)), but the value per cm^3 surpasses that of feature (a) after the surface grinding process allocation (Fig. 8(g)). The bottom bearing surface (c) is the feature with the overall highest impact per cm^3. Similar to the top bearing surface (b), this is the result of compounding environmental impact, allocated across multiple processes. However, in this case, the allocated LCA value exceeds that of the top bearing surface (b) as significantly more value is allocated here during the turning process (Fig. 8(e)). This is due to some of the LCA value for the pre-turning process, which was previously allocated to the outer surface (Fig. 8(d)), being reallocated as the voxels were removed, to the newly formed surface (Fig. 8(e)), in addition to the turning LCA value.

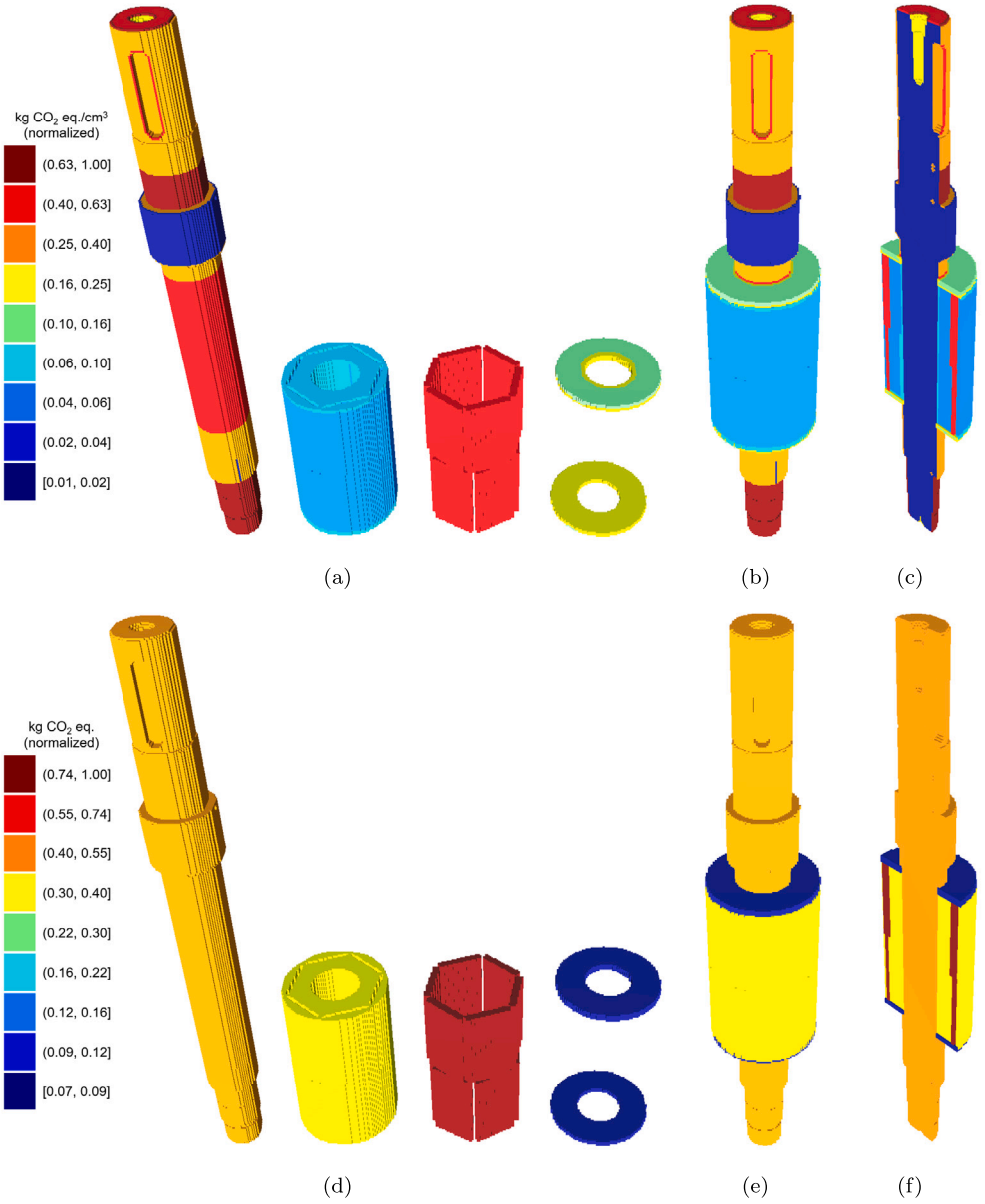

Fig. 7. (a) Feature-level results visualizing global warming impacts per cm^3 across components. (b) Feature-level visualization of results on the sub-assembly. (c) Cross-section view of feature-level results for the sub-assembly. (d) Component-level results showcasing global warming impacts. (e) Component-level visualization of results on the sub-assembly. (f) Cross-section view of component-level results for the sub-assembly. Note that color values are based on the Log_{10} of the voxel values in (a)–(c) and Log_{10} of component values in (d)–(f).

9. Discussions

Fig. 9 shows the LCA results from Table 2 as a bar chart, as they would typically be visualized using current LCA software. These visual representations are designed, and are effective, for communicating results at a unit process level (as in Fig. 9(a)) or at a component-level (as in Fig. 9(b)). However, these representations do not present a clear picture of the associated geometric context. This may not be significant if the intent is to simply understand the overall environmental impacts of a product, component, or the processes involved in producing the product. Nevertheless, providing a geometric context can be critical in other scenarios, e.g., for identifying potential redesign opportunities for a product or component.

Figs. 7(d)–7(f) show a component-level visualization of LCA results similar to Fig. 9(b), while additionally integrating some of the geometric context. However, the added information is minimal and only serves to associate the environmental impact value to the final shape of the component (as opposed to the component name in Fig. 9(b)). It could be argued that, in many ways, this representation is less effective than the bar chart, as LCA values are encoded using color, which is typically perceived less accurately than a bar chart's length (Cleveland and McGill, 1984). Nevertheless, this representation has the benefit of possible integration with CAD software. Designers can view the associated environmental impacts of components in an assembly modeling environment, similar to the concept proposed by Ostad-Ahmad-Ghorabi et al. (2009) and commercial CAD solutions like *Solidworks Sustainability Xpress*. Even so, they do not address a designer's need for understanding which features in a component significantly contribute to its overall impact, and what processes are significantly contributing to the impact of said features. Improving this understanding through more detailed visualizations (e.g., at the feature- or sub-feature-level) can help designers identify new opportunities for sustainable design.

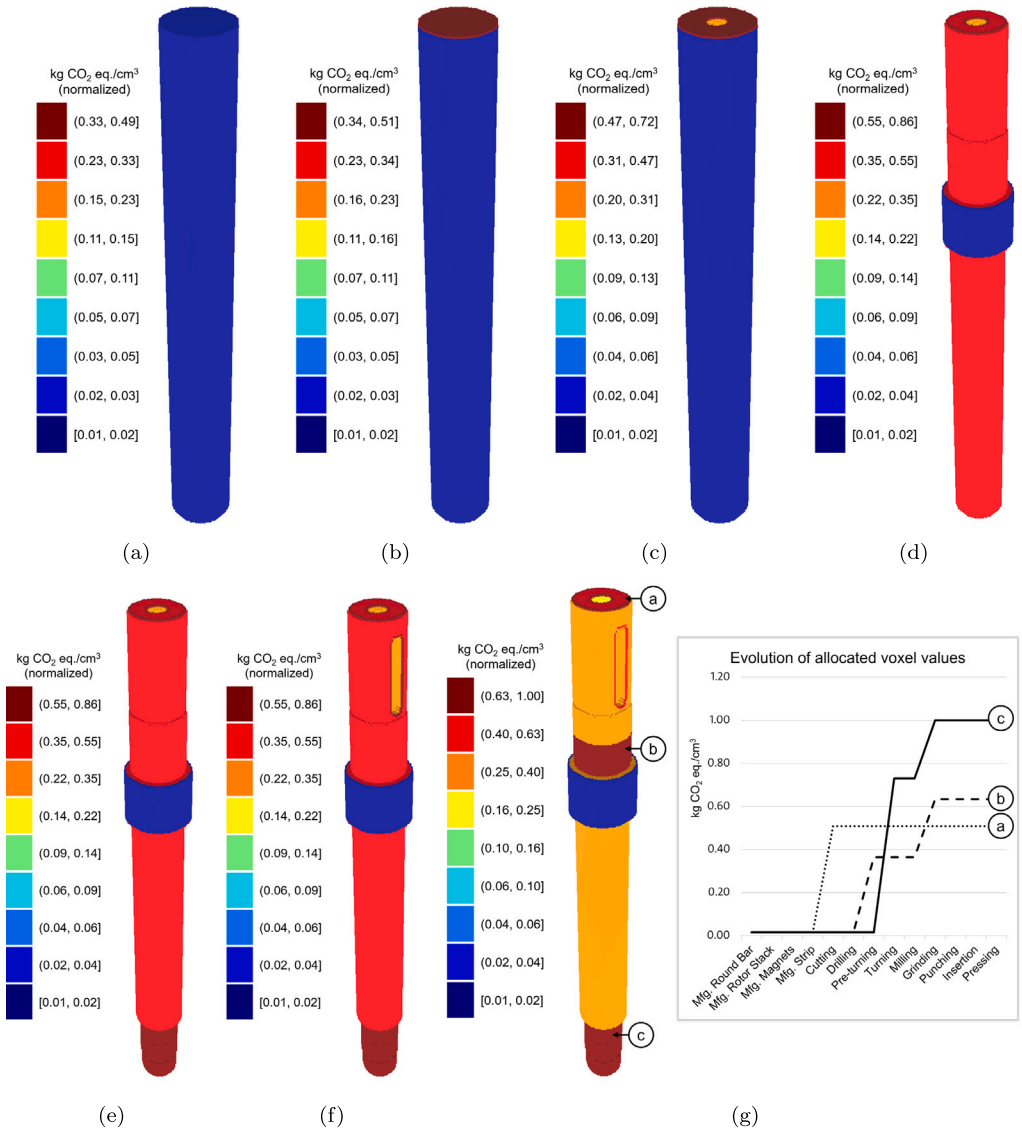

Fig. 8. LCA results sequentially allocated to shaft stages: (a) Round Bar, (b) Cut Shaft, (c) Drilled Shaft, (d) Pre-turned Shaft, (e) Turned Shaft, (f) Milled Shaft, (g) Finished Shaft with a chart showing the evolution of the allocated voxel values across all processes, for three of the highest impact features. Color values are based on the Log_{10} of the normalized voxel values. Please note that the legends change across (a)–(g) as the values allocated to voxels either increase or remain constant over the manufacturing processes.

However, additional aspects need to be considered when evaluating the environmental impacts at this level of detail. For instance, the inherent dependencies between geometric features must be considered when evaluating the impact of a feature. This information is captured in the visualization generated through our proposed methodology and is perhaps most evident in Fig. 8. Here, the bearing surfaces created by the grinding process (Fig. 8(g)) have the highest value of impact per cm^3 in the final representation, despite a low overall impact of the grinding operation itself. This is because the impacts of creating the bearing surfaces are not limited to the grinding process itself. The grinding process removes a negligible quantity of material and prior material removal processes (i.e., turning) are required for surface preparation. Therefore, when evaluating the environmental impacts of creating the bearing surfaces, the impacts of the previous turning processes must be taken into account. In the case of the proposed methodology, the LCA results stored in the corresponding voxels are compounded over the sequence of processes required to obtain the bearing surfaces as shown in Figs. 8(a)–8(g).

Fig. 8 further showcases the value of considering the full geometric context of components for data allocation and visualization. Allocating data at this level of detail, and visualizing results at each intermediate stage can also serve as a history of the part's geometric transformations and can aid designers and manufacturers in understanding the evolution of the environmental impact of the part across the production stages. In doing so, insight can be gained regarding what processes contribute to the total environmental impact of manufacturing a feature, and in what proportion. This insight can be critical for understanding the cause of a feature's impact, and thus help make an informed decision on how to address it.

An important factor in preserving geometric context, and generating physically-accurate visualizations, is the reallocation of the environmental impact of removed voxels, as described in Section 5.2. This is designed to highlight the causal dependency between features, and therefore represent the total environmental burden for generating a given geometric feature or material property. Fig. 10(a) shows the result of allocating the LCA results to the voxels corresponding to the removed material, without subsequently removing them and redistributing the allocated values to neighboring visible voxels. While this is more akin to how LCAs are typically conducted (i.e., environmental impact is computed based on the amount of material removed), it is not

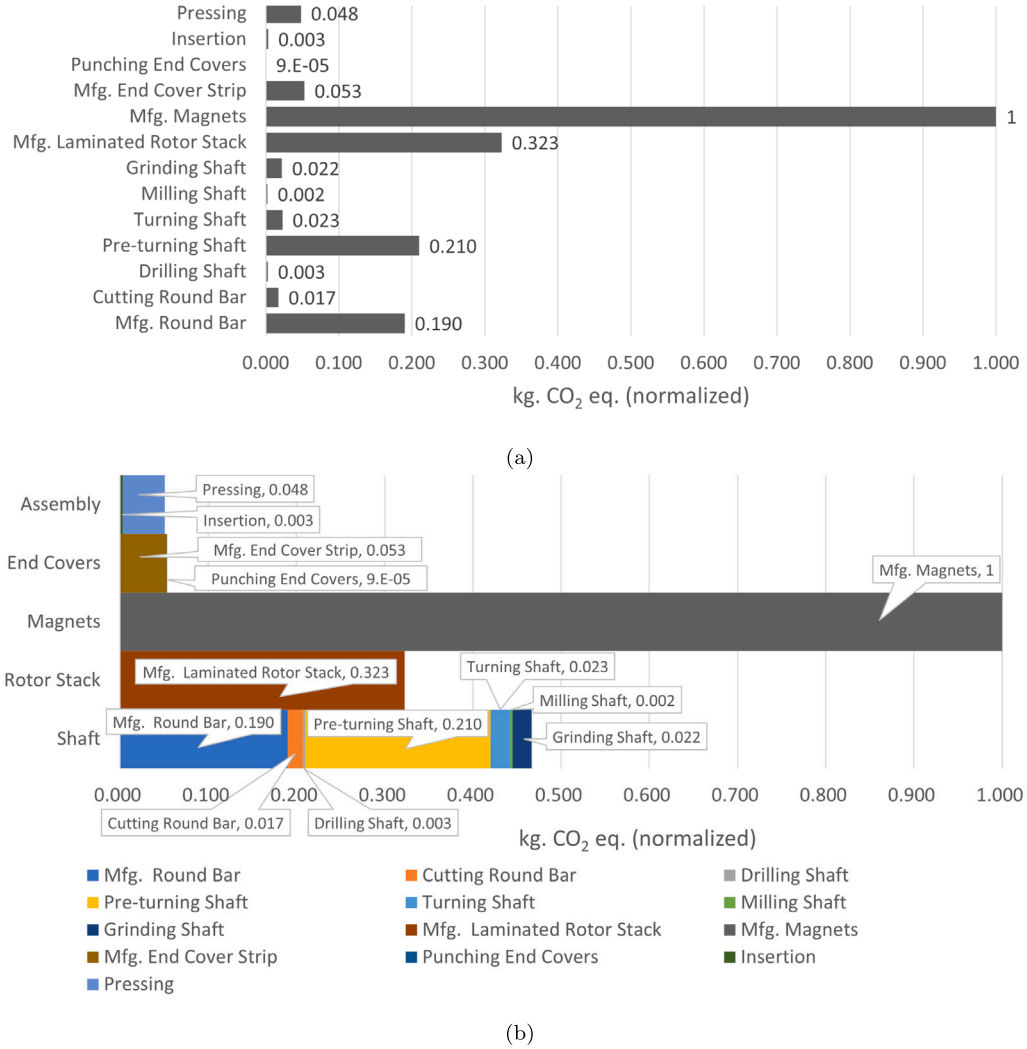

Fig. 9. Normalized LCA results for producing the shaft and rotor sub-assembly visualized, (a) at a unit process-level using a bar graph, and (b) at a component-level using a stacked bar graph.

as useful from a visualization perspective. The results are more difficult to interpret, even with a cross-section view shown in Fig. 10(b). For instance, this representation makes it difficult to differentiate between voxels removed by the pre-turning and turning operations in the final representation. Information regarding causal dependencies between features is also missing. For example, roughly the same value per cm^3 is allocated to the voxels removed by the two processes. This is in line with the computed LCA results but fails to capture, and inform of, the fact that the pre-turning process necessarily has to be performed before the surface created by the turning process can be produced.

The impact of the chosen resolution on the final visualization should also be discussed. The main way in which voxel size can influence the interpretation of the results is if the chosen resolution is not sufficiently high to capture all the relevant features of a component. This means that some features will not be accurately represented in the final model. However, if a sufficiently high resolution is chosen, it would not significantly influence the proposed allocation methodology thereafter. This is because while voxelization errors depend on the chosen resolution (e.g., a lower resolution will result in a coarser approximation of a curved feature), the proposed methodology allocates the LCI/LCA results (e.g., kg. CO_2 eq.) to any visible voxels belong to that specific feature. If the model is at a lower resolution, the results are distributed among fewer voxels. This aspect is essential for keeping the resulting allocation methodology valid. In other words, summing the LCI/LCA results over all individual voxels always matches the results computed through the LCI/LCA study, independent of the chosen voxel resolution. Consequently, the absolute value of LCI/LCA results allocated to voxels will differ with resolution. The absolute value per voxel is inversely proportional to the voxel density/resolution. However, this becomes less of an issue when the values are normalized (i.e., value per cm^3 rather than per voxel) as done throughout this paper. Finally, it is worth noting that the resulting visualization is not meant to interpret absolute values. Traditional visualization schemes, e.g., a bar chart, are more suitable for this task. Rather, the visualization generated through our proposed method highlights proportional differences between regions of the product geometry; this is not significantly affected by the chosen voxel resolution.

It should be mentioned, that in these discussions we do not intend to state that the generated three-dimensional visualizations of LCA results as shown in Fig. 7 are more efficient or useful than traditional LCA visualizations shown in Fig. 9. The two visualization schemes contain different amounts of information and serve different purposes. They should be seen as complementary representations, whose utility depends on the context and the intended audience. For instance, the benefits of our proposed methodology can be limited in cases where the product geometry is simple, or if there are a limited amount of unit processes performed. Nevertheless, as presented in our results and discussions, the mapping and visualization methodology proposed in

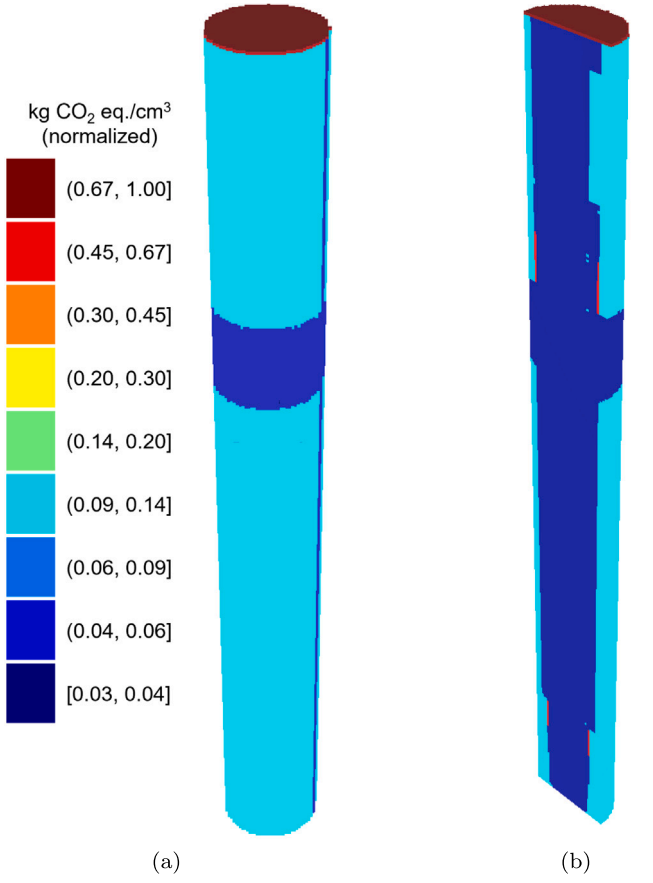

Fig. 10. (a) Visualization of the finished shaft without voxel removal. (b) Cross-section view of the same results.

this work can reduce disparities between data representations currently generated in LCA studies and those useful for design decision-making.

10. Limitations and future directions

Building a voxel-based representation and allocating data according to the proposed methodology requires more information when compared to generating tabular or chart-based visualizations of LCI/LCA results. This is because this methodology combines several input data sources (i.e., CAD models, detailed process plans, and LCI/LCA values) into a common data representation for gaining new insights into feature-level distribution of environmental impacts. Additional effort may also be required to develop CAD models of intermediate product stages if these are not already available or to implement appropriate functions to select the relevant voxel volumes. Further research is required to identify the situations where feature-level visualizations of LCI/LCA provide significant additional benefits. Future work is also required for evaluating the effectiveness of visualizations that can be generated using the proposed methodology and for investigating how uncertainties in LCI/LCA results can be conveyed through the generated three-dimensional visualizations.

It should be noted that errors in the voxelization algorithm can also lead to allocation and visualization errors in the final models. An example of this can be seen in the four points present in the shaft interior in Fig. 7(c). These errors stem from limitations in the voxelization algorithm that resulted in improperly filling the shaft interior with voxels. The resulting holes were interpreted as removed material by our implementation. Therefore a larger amount of impact value was attributed to the neighboring voxels compared to the rest of the shaft interior. However, this is not a limitation of the allocation or visualization methodology, but rather an implementation one. To mitigate these issues, sanity checks should be implemented to ensure the accuracy of the results. One example that was implemented in this work was to verify that the total LCA results value allocated to the model, matches the sum of the values contained in individual voxels. Additionally, it was checked that no data is allocated to invisible voxels. Otherwise, this would lead to a misleading visualization in which not all data is represented.

It should also be reiterated that the presented case study made use of background LCI data, and therefore data was only allocated at a feature-level and assumed to be uniformly distributed across features. However, the methodology allows for a higher granularity of allocation, i.e., at the individual voxel level. Using actual data from the manufacturing process instead of generic data from background databases can open additional opportunities not discussed in this work. However, future work should also investigate the computational requirements for such a detailed allocation and evaluate the necessary level of granularity and the effort required to achieve it.

Finally, while not a limitation of the method itself, it should be noted that the chosen case study does not showcase all classes of processes. Rather, it only illustrates the application of the methodology to the predefined processes involved in the production of the selected sub-assembly. For instance, the case study does not include Class I (e.g., transport) or Class II (e.g., deformation) processes. However, we believe the selected sub-assembly contains sufficient complexity to adequately exemplify the methodology, and other processes could be similarly implemented. As discussed in Section 3, the focus of our work is primarily on visualizing cradle-to-gate impacts for producing mechanical parts having some geometric complexity. Alternate allocation and visualization methodologies should be investigated for integrating LCA/LCI visualization with CAD models for other applications, e.g., electronic components manufacturing and for stakeholders other than mechanical designers.

11. Conclusions

This paper presented a methodology for mapping LCI/LCA data to part features through the use of voxel-based representations. The developed methodology enables three-dimensional visualizations of LCI/LCA data in the context of the part's geometry, in an attempt to bridge the gap between data representations used for design, manufacturing, and LCA. Bridging this gap can facilitate communication of LCA results to relevant stakeholders by relating the results to data representations and visualizations typically used by design engineers and manufacturers. The data allocation methodology was demonstrated through a case study involving a *shaft and rotor* sub-assembly and exemplified the generation of three-dimensional, component- and feature-level, visualizations. Importantly, the developed methodology preserves the context of intermediate changes in part geometry, rather than only considering, and allocating data to the finished component. This context can be critical for understanding causal dependencies between part features, which need to be taken into account for redesigning components and geometric features. Compared to previous efforts, the allocation methodology enables the visualization of LCI/LCA data at a higher granularity level, including feature-, and sub-feature-level. Through this work, we hope to contribute to better understanding, communication and integration of environmental impact results in the design and manufacturing stages, leading to cleaner and more sustainable production.

CRediT authorship contribution statement

Teodor Vernica: Conceptualization, Methodology, Investigation, Software, Validation, Visualization, Writing – original draft. **Marija Glišić:** Investigation, Data curation, Writing – original draft. **Badrinath**

Veluri: Resources, Supervision, Writing – review & editing, Project administration. **Devarajan Ramanujan:** Supervision, Conceptualization, Methodology, Writing – review & editing, Project administration, Funding acquisition.

Declaration of competing interest

The authors declare the following financial interests/personal relationships which may be considered as potential competing interests: Devarajan Ramanujan reports that financial support for conducting this research work was provided by Grundfos Holding. The contents and results reported in this manuscript reflect the authors independent findings and were not influenced or edited in any manner by the funding agency.

Data availability

The data that has been used is confidential.

Acknowledgments

The authors would like to thank Dr. Vinayak Krishnamurthy and Dr. Senthil Chandrasegaran for their feedback on the manuscript. This work is partially supported by funding from the Grundfos Advanced Manufacturing Engineering division, Denmark. This paper represents original findings and opinions of the authors. No official recommendation or endorsement of the presented work is implied by Grundfos A/S.

Appendix A. Supplementary data

Supplementary material related to this article can be found online at https://doi.org/10.1016/j.jclepro.2023.138035.

References

Bernstein, W., Ramanujan, D., Devanathan, S., Zhao, F., Ramani, K., Sutherland, J.W., 2010. Development of a framework for sustainable conceptual design. In: Proceedings of the 17th CIRP International Conference on Life Cycle Engineering.

Bernstein, W.Z., Ramanujan, D., Kulkarni, D.M., Tew, J., Elmqvist, N., Zhao, F., Ramani, K., 2015. Mutually coordinated visualization of product and supply chain metadata for sustainable design. J. Mech. Des. 137 (12).

Bernstein, W.Z., Tensa, M., Praniewicz, M., Kwon, S., Ramanujan, D., 2020. An automated workflow for integrating environmental sustainability assessment into parametric part design through standard reference models. Procedia CIRP 90, 102–108. http://dx.doi.org/10.1016/j.procir.2020.02.058, URL https://www.sciencedirect.com/science/article/pii/S2212827120301839. 27th CIRP Life Cycle Engineering Conference (LCE2020)Advancing Life Cycle Engineering : from technological eco-efficiency to technology that supports a world that meets the development goals and the absolute sustainability.

Boettjer, T., Thoft Krogshave, J., Ramanujan, D., 2021. Machine-specific estimation of milling energy consumption in detailed design. J. Manuf. Sci. Eng. 143 (8).

Cerdas, F., Kaluza, A., Erkisi-Arici, S., Böhme, S., Herrmann, C., 2017. Improved visualization in LCA through the application of cluster heat maps. Procedia Cirp 61, 732–737.

Chandru, V., Manohar, S., Prakash, C.E., 1995. Voxel-based modeling for layered manufacturing. IEEE Comput. Graph. Appl. 15 (6), 42–47.

Chang, D., Lee, C., Chen, C.-H., 2014. Review of life cycle assessment towards sustainable product development. J. Clean. Prod. 83, 48–60.

Chen, X., Griffin, W.M., Matthews, H.S., 2018. Representing and visualizing data uncertainty in input-output life cycle assessment models. Resour. Conserv. Recy. 137, 316–325.

Cleveland, W.S., McGill, R., 1984. Graphical perception: Theory, experimentation, and application to the development of graphical methods. J. Amer. Statist. Assoc. 79 (387), 531–554.

Elbeltagi, E., Wefki, H., Abdrabou, S., Dawood, M., Ramzy, A., 2017. Visualized strategy for predicting buildings energy consumption during early design stage using parametric analysis. J. Build. Eng. 13, 127–136.

Gaha, R., Benamara, A., Yannou, B., 2018. Proposition of eco-feature: a new CAD/PLM data model for an LCA tool. In: Design and Modeling of Mechanical Systems—III: Proceedings of the 7th Conference on Design and Modeling of Mechanical Systems, CMSM'2017, March 27–29, Hammamet, Tunisia 7. Springer, pp. 763–770.

Gutiérrez, E., Lozano, S., Adenso-Díaz, B., 2010. Dimensionality reduction and visualization of the environmental impacts of domestic appliances. J. Ind. Ecol. 14 (6), 878–889.

Hajibabai, L., Aziz, Z., Peña-Mora, F., 2011. Visualizing greenhouse gas emissions from construction activities. Constr. Innov. 11 (3), 356–370.

Heijungs, R., 2014. Ten easy lessons for good communication of LCA.

Hollberg, A., Kiss, B., Röck, M., Soust-Verdaguer, B., Wiberg, A.H., Lasvaux, S., Galimshina, A., Habert, G., 2021. Review of visualising LCA results in the design process of buildings. Build. Environ. 190, 107530.

Huijbregts, M.A., Steinmann, Z.J., Elshout, P.M., Stam, G., Verones, F., Vieira, M., Hollander, A., Zijp, M., van Zelm, R., 2016. ReCiPe 2016: a harmonized life cycle impact assessment method at midpoint and endpoint level report I: characterization.

International Organization for Standardization, 2006. Environmental Management - Life Cycle Assessment - Principles and Framework. Standard No. ISO 14040:2006, International Organization for Standardization, Geneva, Switzerland, https://www.iso.org/standard/37456.html.

Jense, G., 1989. Voxel-based methods for CAD. Comput. Aided Des. 21 (8), 528–533.

Kaufman, A., Cohen, D., Yagel, R., 1993. Volume graphics. Computer 26 (7), 51–64.

Lupton, R.C., Allwood, J.M., 2017. Hybrid sankey diagrams: Visual analysis of multidimensional data for understanding resource use. Resour. Conserv. Recy. 124, 141–151.

MacEachren, A., Xiping, D., Hardisty, F., Guo, D., Lengerich, G., 2003. Exploring high-d spaces with multiform matrices and small multiples. In: IEEE Symposium on Information Visualization 2003 (IEEE Cat. No. 03TH8714). IEEE, pp. 31–38.

Maruschke, J., Rosemann, B., 2005. Measuring environmental performance in the early phases of product design using life cycle assessment. In: 2005 4th International Symposium on Environmentally Conscious Design and Inverse Manufacturing. pp. 248–249. http://dx.doi.org/10.1109/ECODIM.2005.1619214.

Meißner, M., Pfister, H., Westermann, R., Wittenbrink, C.M., 2000. Volume visualization and volume rendering techniques. In: Eurographics (Tutorials).

Michiels, F., Geeraerd, A., 2020. How to decide and visualize whether uncertainty or variability is dominating in life cycle assessment results: A systematic review. Environ. Model. Softw. 133, 104841.

Müller, D.P., Hiete, M., 2021. Visualization supported corporate decision making for life cycle sustainability assessment–Illustrated using a case study for selecting a sustainable packaging system for self-leveling compounds. J. Clean. Prod. 313, 127768.

Newman, T.S., Yi, H., 2006. A survey of the marching cubes algorithm. Comput. Graph. 30 (5), 854–879.

Ostad-Ahmad-Ghorabi, H., Collado-Ruiz, D., Wimmer, W., 2009. Towards integrating LCA into CAD. In: DS 58-7: Proceedings of ICED 09, the 17th International Conference on Engineering Design, Vol. 7, Design for X/Design To X, Palo Alto, CA, USA, 24.-27.08. 2009.

Otto, H.E., Mueller, K.G., Kimura, F., 2003. Efficient information visualization in LCA: Introduction and overview. Int. J. Life Cycle Assess. 8, 183–189.

Otto, H.E., Mueller, K.G., Kimura, F., 2004. LCA related interactive knowledge visualisation for product design. In: Knowledge Intensive Design Technology: IFIP TC5/WG5. 2 Fifth Workshop on Knowledge Intensive CAD July 23–25, 2002, St. Julians, Malta. Springer, pp. 81–96.

Patil, S., Ravi, B., 2005. Voxel-based representation, display and thickness analysis of intricate shapes. In: Ninth International Conference on Computer Aided Design and Computer Graphics (CAD-CG'05). IEEE, p. 6.

Prado, V., Seager, T.P., Guglielmi, G., 2022. Challenges and risks when communicating comparative LCA results to management. http://dx.doi.org/10.1007/s11367-022-02090-5.

Ramanujan, D., Bernstein, W.Z., Chandrasegaran, S.K., Ramani, K., 2017a. Visual analytics tools for sustainable lifecycle design: Current status, challenges, and future opportunities. J. Mech. Des. 139 (11), 111415. http://dx.doi.org/10.1115/1.4037479.

Ramanujan, D., Bernstein, W.Z., Ramani, K., 2017b. Design patterns for visualization-based tools in sustainable product design. In: 22nd Design for Manufacturing and the Life Cycle Conference; 11th International Conference on Micro- and Nanosystems of International Design Engineering Technical Conferences and Computers and Information in Engineering Conference. Vol. 4, V004T05A042. http://dx.doi.org/10.1115/DETC2017-68054.

Raoufi, K., Harper, D.S., Haapala, K.R., 2020. Reusable unit process life cycle inventory for manufacturing: metal injection molding. Prod. Eng. 14 (5), 707–716.

Raoufi, K., Taylor, C., Laurin, L., Haapala, K.R., 2019. Visual communication methods and tools for sustainability performance assessment: linking academic and industry perspectives. Procedia CIRP 80, 215–220.

Reap, J., Roman, F., Duncan, S., Bras, B., 2008. A survey of unresolved problems in life cycle assessment: Part 2: Impact assessment and interpretation. Int. J. Life Cycle Assess. 13, 374–388.

Resch, E., Lausselet, C., Brattebø, H., Andresen, I., 2020. An analytical method for evaluating and visualizing embodied carbon emissions of buildings. Build. Environ. 168, 106476.

Rio, M., Blondin, F., Zwolinski, P., 2019. Investigating product designer LCA preferred logics and visualisations. Procedia CIRP 84, 191–196.

Rio, M., Reyes, T., Roucoules, L., 2013. Toward proactive (eco)design process: modeling information transformations among designers activities. J. Clean. Prod. 39, 105–116. http://dx.doi.org/10.1016/j.jclepro.2012.07.061, URL https://www.sciencedirect.com/science/article/pii/S0959652612004131.

Röck, M., Hollberg, A., Habert, G., Passer, A., 2018a. LCA and BIM: Integrated assessment and visualization of building elements' embodied impacts for design guidance in early stages. Procedia CIRP 69, 218–223.

Röck, M., Hollberg, A., Habert, G., Passer, A., 2018b. LCA and BIM: Visualization of environmental potentials in building construction at early design stages. Build. Environ. 140, 153–161.

Saidani, M., Pan, E., Kim, H., 2020. Switching from petroleum-to bio-based plastics: visualization tools to screen sustainable material alternatives during the design process. In: International Design Engineering Technical Conferences and Computers and Information in Engineering Conference, Vol. 83952. American Society of Mechanical Engineers, V006T06A030.

Scheve, M., de Vlieg, J., Geurts, F., 2022. Impact landscapes: Supporting the interpretation and communication of life cycle assessments with interactive voronoi treemaps.

Sorensen, D.G., Brunø, T.D., Nielsen, K., 2018. A classification scheme for production system processes. Procedia CIRP 72, 609–614.

Tao, J., Chen, Z., Yu, S., Liu, Z., 2017. Integration of life cycle assessment with computer-aided product development by a feature-based approach. J. Clean. Prod. 143, 1144–1164.

Tao, J., Li, L., Yu, S., 2018. An innovative eco-design approach based on integration of LCA, CAD\ CAE and optimization tools, and its implementation perspectives. J. Clean. Prod. 187, 839–851.

Telea, A., Jalba, A., 2011. Voxel-based assessment of printability of 3D shapes. In: Mathematical Morphology and Its Applications To Image and Signal Processing: 10th International Symposium, ISMM 2011, Verbania-Intra, Italy, July 6-8, 2011. Proceedings 10. Springer, pp. 393–404.

Téno, J.-F.L., 1999. Visual data analysis and decision support methods for non-deterministic LCA. Int. J. Life Cycle Assess. 4, 41–47.

Thoft Krogshave, J., Boettjer, T., Ramanujan, D., 2020. Machine-specific energy estimation using the unit process life cycle inventory (UPLCI) model. In: Proceedings of the ASME 2020 International Design Engineering Technical Conferences. Virtual, Online. August 17–19. American Society of Mechanical Engineers Digital Collection, V006T06A031.

Uchil, P., Chakrabarti, A., 2013. Communicating life cycle assessment results to design decision makers: Need for an infomration visualization approach. In: DS 75-5: Proceedings of the 19th International Conference on Engineering Design (ICED13) Design for Harmonies, Vol. 5: Design for X, Design To X, Seoul, Korea 19-22.08. 2013.

Wiberg, A.H., Wiik, M.K., Auklend, H., Slåke, M.L., Tuncer, Z., Manni, M., Ceci, G., Hofmeister, T., 2019. Life cycle assessment for zero emission buildings–a chronology of the development of a visual, dynamic and integrated approach. In: IOP Conference Series: Earth and Environmental Science, Vol. 352. IOP Publishing, 012054.

Xue, J., Zhao, G., Xiao, W., 2016. Efficient GPU out-of-core visualization of large-scale CAD models with voxel representations. Adv. Eng. Softw. 99, 73–80.